Molecular Simulation of the DMPC-Cholesterol Phase Diagram

Frédérick J.-M. de Meyer,*,†,‡ Ayelet Benjamini,‡,§ Jocelyn M. Rodgers,‡ Yannick Misteli,†,∥ and Berend Smit†,‡,§

Department of Chemical Engineering, University of California, Berkeley, 101B Gilman Hall, Berkeley, California 94720-1462, Materials Science Division, Lawrence Berkeley National Laboratory, Berkeley, California 94720, Department of Chemistry, University of California, Berkeley, 101B Gilman Hall, Berkeley, California 94720-1462, and Department of Computer Science, ETH Zürich, Switzerland

Received: April 29, 2010; Revised Manuscript Received: July 11, 2010

In this paper, we present a coarse-grained model of a hydrated saturated phospholipid bilayer (dimyristoylphosphatidylcholine, DMPC) containing cholesterol that we study using a hybrid dissipative particle dynamics−Monte Carlo method. This approach allows us to reach the time and length scales necessary to study structural and mechanical properties of the bilayer at various temperatures and cholesterol concentrations. The properties studied are the area per lipid, condensation, bilayer thickness, tail order parameters, bending modulus, and area compressibility. Our model quantitatively reproduces most of the experimental effects of cholesterol on these properties and reproduces the main features of the experimental phase and structure diagrams. We also present all-atom simulation results of the system and use these results to further validate the structure of our coarse-grained bilayer. On the basis of the changes in structural properties, we propose a temperature−composition structure diagram, which we compare with the experimental phase and structure diagrams. Attention is paid to the reliability and interpretation of the model and simulation method and of the different experimental techniques. The lateral organization of cholesterol in the bilayer is discussed.

Introduction

Experiments in vitro and in vivo, performed to gain insight into the exact role of cholesterol in membranes, revealed its complexity.[1] Even for the extensively studied hydrated bilayer containing solely cholesterol and dimyristoylphosphatidylcholine (DMPC), the effect of cholesterol is not entirely understood.[2] In fact, as shown in Figure 1, there is even no consensus on the qualitative form of the cholesterol−DMPC phase diagrams in the literature.

By definition, if a sudden change in the enthalpy of the system takes place, for example, as a function of temperature at constant pressure, a phase transition occurs. One of the most widely used methods to measure phase transitions of lipid membranes is differential scanning calorimetry (DSC).[3−5] With DSC, however, it is not possible to characterize the structural, mechanical, or dynamical properties of the bilayer in a given phase or to determine which forces drive the phase transition.[3] Several experimental methods to gain information on the structural, mechanical, and dynamical properties of a bilayer exist. For example, from NMR and X-ray scattering data, one can extract lipid tail order parameters;[6] from X-ray scattering one obtains electron density profiles, bilayer thickness, bending modulus, and area per lipid;[7,8] and from fluorescence techniques and NMR, diffusion coefficients can be obtained.[9−11]

The available experimental methods can either directly determine the phase boundaries (DSC) or yield information on structural, mechanical, or dynamical changes (NMR, X-ray, fluorescence). Therefore, the comparison between the phase diagram and the different diagrams showing structural, mechanical, or dynamical changes is not straightforward. Moreover, the different experimental techniques may not be sensitive to all changes that are induced by cholesterol. Molecular simulations should, in principle, allow one to simultaneously obtain information concerning a broad range of bilayer properties.

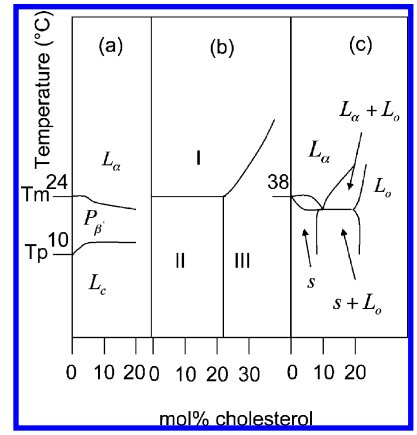

Figure 1. Published partial phase diagrams of a hydrated DMPC−cholesterol bilayer. T_M and T_P are the main and the pretransition temperatures of the pure DMPC bilayer, respectively. In (a), obtained from small-angle neutron scattering experiments which give information on the ripple structure,[73] L_α is the liquid phase, $P_{\beta'}$ is the ripple phase, and L_c is the non-rippled gel phase. In (b), obtained from differences in membrane fluidity, observed using paramagnetic resonance spectra spin-labels,[74] region I denotes the liquid phase which can eventually contain two liquid−liquid immiscible regions; region II denotes a solid phase−fluid phase phase separation; and region III denotes a single-phase fluid region. In (c), which is a DPPC−cholesterol phase diagram obtained from DSC measurements and NMR,[58] s and L_o are the solid phase and the liquid-ordered phase, respectively.

Using all-atom molecular dynamic simulations, many effects of cholesterol have been studied on several types of lipid

* To whom correspondence should be addressed. E-mail: frederickdemeyer@berkeley.edu. Tel.: +1 (510) 642 9275. Fax: +1 (510) 642 8063.
† UC Berkeley, Chemical Engineering.
‡ Lawrence Berkeley National Laboratory.
§ UC Berkeley, Chemistry.
∥ ETH Zürich.

10.1021/jp103903s
Published on Web 07/26/2010

bilayers.[7,12−17] The ordering and condensation effects have been observed in simulations of DPPC/Chol and DMPC/Chol mixtures.[7,13−15] The study was extended to different types of sterols and also to bilayers containing sphingomyelin.[15,18] Pandit et al.[7] studied the packing of cholesterol around unsaturated lipids. Kucerka et al.[16] used molecular simulations to relate the simulated bilayer structure to experimental X-ray results thereby allowing a detailed comparison to the experimental models. Earlier studies[13,19−25] used a united-atom model to investigate the impact of cholesterol and other sterol molecules on lipid bilayers. These studies use effectively less atoms by grouping a few of the atoms together. Those simulations obtain similar trends for the effect of cholsterol and other sterols. Pasenkiewicz-Gierula et al.[13,21,22] used those simulations to distinguish between the different types of cholesterol interactions. An extensive study by Hofsass et al.[25] followed the effect of cholesterol on the properties of a DPPC bilayer at various concentrations.

Unfortunately, the length scales (1−1000 nm) and time scales (1−1000 ns) required to study phase transitions of atomistic lipid models are simply not accessible with current computers. Very extensive simulations are required to reliably determine the phase boundaries, and therefore even a single-phase point requires much more resources than one has. To access the necessary length and time scales, various coarse-grained models of lipid bilayers have been developed.[26] A popular method to study the structure, mechanics, and dynamics of coarse-grained lipid bilayers is dissipative particle dynamics (DPD).[27] This approach has been successful in reproducing various structural properties of the different phases of a single phospholipid bilayer.[26,28] Recently, coarse-grained models of lipid bilayers containing cholesterol have been developed.[29−32] Murtula et al.[30] studied the lateral organization of cholesterol at intermediate cholesterol concentrations, while Marrink et al.[31] reproduced the condensation effect of cholesterol.

In a previous article,[32] we presented a coarse-grained model of DMPC and cholesterol, and we studied the physical mechanism of cholesterol condensation. We investigated how the condensation effect depends on the main structural aspects of cholesterol by comparing the effect of cholesterol with the effect of other alcohols. In this article,[32] we also presented some preliminary data on the phase diagram of cholesterol in DMPC. In the present article we build upon these results and present a more complete phase diagram. In addition, we make a detailed comparison of our coarse-grained simulations with experimental data and all-atom simulations.

In the present article, we first validate this coarse-grained model of DMPC and cholesterol further—using all-atom simulations, exploring more properties, and making a more extensive comparison with experiments. We study the effect of cholesterol concentration and temperature on the structure and mechanics of the phospholipid bilayer and on the lateral organization of cholesterol. We determine different structural transitions of the system more systematically and construct a temperature−composition structure diagram which we compare with the available experimental temperature−composition phase and structure diagrams. The simulations performed in this paper were in the $NP_{\perp}\gamma T$ ensemble to allow variable hydration of the lipid head groups and closer relations to experimental conditions, compared to the simulations in the $NV\gamma T$ ensemble used in the article on cholesterol condensation.[32]

Model and Simulation Method

We adopted a mesoscopic representation of the molecular components of the system, namely, water, lipid, and cholesterol,

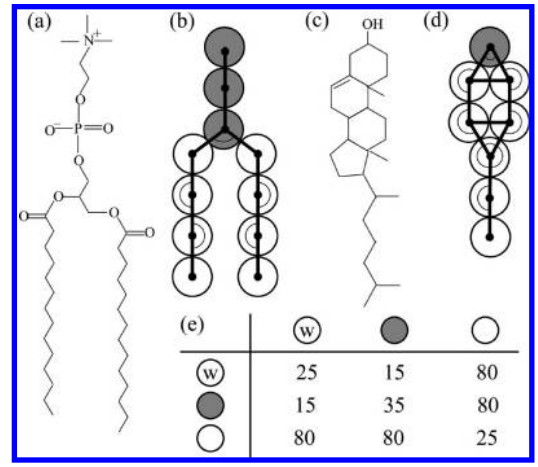

Figure 2. Molecular structure and mesoscopic model of DMPC (a, b) and cholesterol (c, d). The hydrophilic and hydrophobic beads are depicted in black and white, respectively. Angles restricted by a harmonic bending potential are specified. In Table (e) the values of the soft-repulsive parameters a_{ij} are given.

where the mean molecular structure, hydrophobic interactions, hydrophobic mismatch, and the flexibility of the components are taken into consideration. Three types of beads are used: a water-like bead (w), a hydrophilic bead, which models a part of a head group of either the lipid or the cholesterol, and a hydrophobic bead, which is used to model a part of either the lipid hydrocarbon tail or the tetrameric ring and acyl chain of the cholesterol (see Figure 2).

In our model, we explicitly assume that hydrophobic mismatch between the cholesterol and the lipid hydrophobic tails is an important parameter regulating the cholesterol−lipid interactions.[5,33−35] In this cholesterol model, we have chosen the parameters and number of beads such that the relative lengths of the different hydrophilic and hydrophobic parts of the cholesterol molecule are consistent with our lipid model.

At this point, it is important to mention that there is no consensus on the values of these parameters. Molecular simulations[22] and simple molecular models show that the hydrophobic length of a single cholesterol molecule is comparable with the hydrophobic length of a single DMPC molecule and that the length of the cholesterol tetrameric ring is comparable with the length of the cholesterol tail. Experiments by McMullen et al.[5] point out that, in a phospholipid bilayer, the total hydrophobic part of cholesterol matches with the length of a phospholipid tail containing 17 carbon atoms, i.e., 17.5 Å. DMPC, which contains a tail of 14 carbon atoms, should hence have a hydrophobic part that is 3−4 Å shorter than the hydrophobic part of cholesterol. We chose a cholesterol model in which the hydrophobic length is slightly longer than the DMPC tail length and in which the length of the cholesterol ring is equal to the length of the cholesterol tail.

In the phospholipid model, one hydrophobic bead represents three to four carbon atoms. To ensure that the effective volume of a cholesterol molecule is consistent with the lipid models, we assume that the cholesterol tail is represented by two beads and that the stiff tetrameric ring is represented by five beads. The five methyl groups are not directly represented in our model. Our model gives a temperature-independent area per cholesterol value of 40.3 Å^2, which is in excellent agreement with the most recent experimental value of 41 Å^2 for a cholesterol monolayer.[36]

At this point, it is important to notice that both the cholesterol and DMPC models are very simple and may thus represent a large variety of sterols and lipids. Experiments and all-atom

molecular simulations indicate that the main effects of a sterol on a saturated lipid bilayer are independent of the type of sterol but that the degree to which a given sterol perturbs a lipid bilayer varies.[18,20,37,38] As a result, the models used in this simulation study can mainly extract general effects of cholesterol on the DMPC structures.

The hydrophobic and hydrophilic interactions are modeled with soft-repulsive potentials, the strengths of which are shown in Figure 2. The energy parameter a_{ww} has been fitted such that the coarse-grained water has the same compressibility as water at ambient conditions.[27] It has been shown that the other energy parameter values can be linked to Flory−Huggins solubility parameters.[27] To be fully correct, these parameters should be refit at each temperature. However, we have found it fruitful to hold these parameters constant to explore the phase behavior in the vicinity of the ambient temperature of 24 °C. As a result, the connection between the coarse-grained temperature, T_r, and real temperature, T, is less well-defined than for the properties related to density. To relate these temperatures, we use the empirical estimate that $T = 108.75T_r - 8.6$, with T_r the reduced temperature, a relationship that was obtained by fitting to the phase transition temperatures. Harmonic bond and bond-bending potentials control the structure and the flexibility of the molecules (see Supporting Information).

The mesoscopic model was studied with the DPD simulation technique.[27,39,40] Since unconstrained lipid bilayers are essentially in a tensionless state,[41] we reproduced this condition by simulating the system in the $NP_\perp\gamma T$ ensemble, where γ is the surface tension of the lipid bilayer, set to zero. We simulate this ensemble via a hybrid Monte Carlo (MC) and dissipative particle dynamics (DPD) approach. Each cycle of the simulation consists of one of the following possible moves: (1) a DPD trajectory of 1−50 steps which applies a thermostat to the dynamics, (2) a constant surface tension MC move, and (3) a constant normal pressure MC move. These moves are chosen with a likelihood of 60%/20%/20%, respectively. For a detailed description of the simulation method and its applications, we refer to the Supporting Information and to previous articles.[42−45]

To minimize finite-size effects, a sufficiently large bilayer patch should be simulated. We have performed simulations on several bilayers which contained 400, 1000, and 4000 molecules. Differences between simulation results of the bilayers containing 400, 1000, and 4000 molecules were found to be minimal. Hence we performed our systematic study on bilayers which contain 400 molecules, and the results presented in this article should barely be subjected to finite-size effects. Because the phase behavior of a lipid bilayer strongly depends on the level of hydration, it is important to ensure sufficient hydration. Moreover, phase transitions might occur with a change of the local hydration of the bilayer.[46] Therefore, we considered 25 water beads per lipid or cholesterol. The simulation in the $NP_\perp\gamma T$ ensemble allows for local changes in the hydration of the bilayer head groups. The normal component of the stress tensor, $P_\perp$, is equal to the bulk pressure of the water phase. This pressure is usually kept constant in the experiments. Previously,[32] this model has been studied at $NV\gamma T$ conditions. Differences between $NV\gamma T$ and $NP_\perp\gamma T$ were found to be minor for this particular system.

We performed simulations of bilayers with different cholesterol concentrations ranging from 0 to 50 mol % at dimensionless temperatures ranging from 0.1 to 1.0. The pure bilayer can be obtained from a self-assembly process. For this study, we generated an initial bilayer in which cholesterol was incorporated by randomly replacing a lipid molecule by a cholesterol molecule in such a way that the total number of lipid and cholesterol molecules on both sides of the membrane is equal. Bennett et al.[24] observed a flip-flop of cholesterol between the two bilayer sides. We did not observe this.

All-atom MD simulations on bilayers composed of DMPC and cholesterol were used for quantitative comparison. A membrane of 72 molecules in total (DMPC and cholesterol) was assembled using the CHARMM-GUI input generator.[47] The replacement method for membrane building was used. An initial constrained equilibration was performed according to the scheme provided by CHARMM-GUI.[48] An equal number of cholesterol molecules were inserted into both leaflets of a DMPC membrane. Three-dimensional periodic boundary conditions were enforced, and a hydration layer of 30 TIP3P water molecules per lipid was used to reduce the mutual influence of images in the direction normal to the bilayer. An initial area of 60 Å^2 per DMPC molecule was set for lower cholesterol concentrations (<20%), while at higher cholesterol concentrations this value was reduced to 50 Å^2. Both the initial energy minimization and the longer MD simulations were performed using the CHARMM package[49] with the optimized lipid parameters.[50] At this point it is important to mention that our all-atom simulations are relatively small. Such small systems are sufficient to obtain accurate data on the structural properties and allow us to compute these properties for many different cholesterol concentrations. However, larger bilayers are required to obtain mechanical parameters or to study cholesterol clustering.

The MD simulations were performed using the leapfrog Verlet integrator over a time step of 2 fs. A temperature of 30 °C was kept constant throughout the simulation as well as constant normal pressure (1 atm) and surface tension (0 dyn/cm), therefore sampling at the $NP_\perp\gamma T$ ensemble. The nonbonded van der Waals interactions were smoothed by a switching function between 10 and 12 Å. The particle mesh Ewald[51] method was used to calculate the long-range interactions beyond this cutoff. Bonds involving hydrogen atoms were kept fixed using the SHAKE algorithm with a tolerance of 10^{-6}. An initial 500 ps minimization was performed according to the scheme provided in CHARMM-GUI.[47] Statistical averages were then obtained from a nanosecond trajectory following 3.5 ns of equilibration.

Results

Comparison with Mechanical and Structural Properties at 30 °C. First, we test our model by a detailed comparison with the experimental data on the effect of cholesterol on various structural and mechanical properties of the bilayer with our simulation results using both all-atom and mesoscopic simulations. Most of these experiments were performed at 30 °C, right above the main transition temperature of pure DMPC, which is 24 °C. We also compare with the data obtained by all-atom simulations, as a further validation of the coarse-grained model.

Structural. Figure 3a shows our simulation results for the average molecular area, A_M, as a function of cholesterol composition together with the experimental data, which have been extracted from X-ray scattering experiments.[8,52] The all-atom simulations reproduce the experimental data very well. For pure DMPC, our mescopic model gives a slightly smaller area. Figure 3a shows that experimentally a nonlinear decrease of the area per molecule as a function of cholesterol concentration is observed. The A_M is smaller than the A_M calculated from the mixing rule. This nonideal mixing behavior is called the condensation effect of cholesterol. Both all-atom and molecular simulations correctly predict the nonlinear decrease of the area per molecule as a function of cholesterol concentration.

Figure 3b shows the relative increase in bilayer thickness in the presence of cholesterol. Experimentally, X-ray scattering

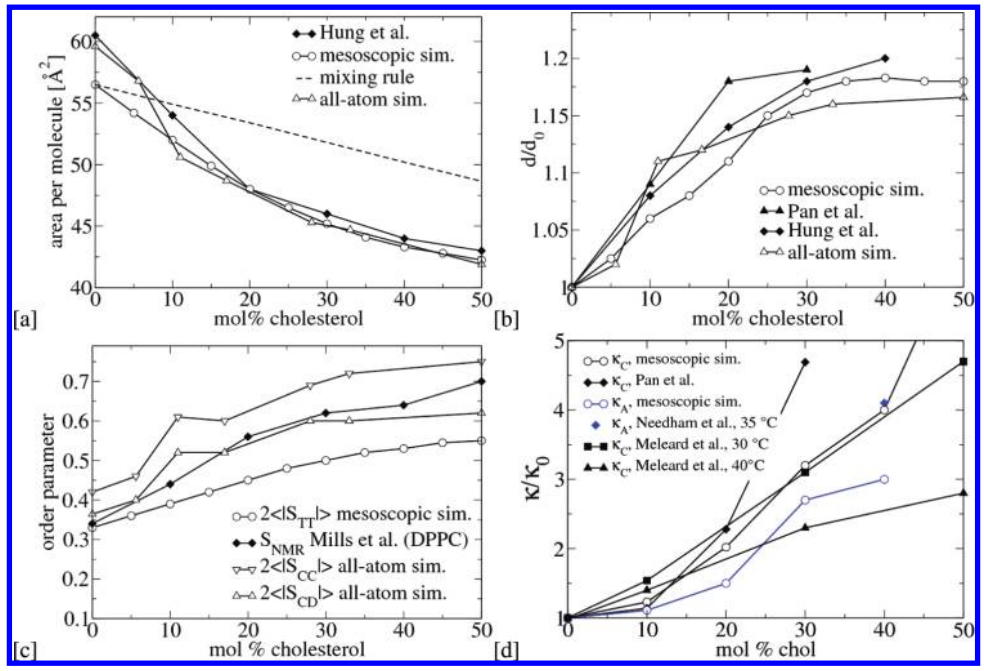

Figure 3. Comparison of structural and mechanical parameters as a function of cholesterol concentration obtained from X-ray scattering experiments (unless specified) and all-atom and mesoscopic simulations. All data are at 30 °C (unless specified). (a) Area per molecule, A_m. Experimental data from Hung et al.[52] The dotted line represents the area per molecule calculated with the mixing rule. (b) Relative bilayer thickness, d/d_0. Experimental data from Hung et al.[52] and Pan et al.[7] d is the phosphorus to phosphorus distance in the electron density profile, and d_0 is the thickness of the pure bilayer. (c) Lipid tail order parameter. Experimental data from Mills et al.[6] Illustration of the qualitative agreement between S_{CC} and S_{CH} using all-atom simulations and comparison to S_{TT} from mesoscopic simulations. (d) Relative bending modulus, κ_C/κ_{C0}, and relative area compressibility modulus, κ_A/κ_{A0}. Experimental data from Pan et al.[7] and from Meléard et al.,[67] extracted from fluctuations of giant vesicles observed by microscope, and from Needham et al.,[54] obtained from pipet pressurization. κ_C is the bending modulus, and κ_{C0} is the bending modulus of the pure bilayer. κ_A is the area compressibility modulus, and κ_{A0} is the area compressibility modulus of the pure bilayer.

provides the phosphorus to phosphorus distance (PtP) as a measure of this thickness.[8,52] We used the same definition in our all-atom simulations. For our mesoscopic model, we used the average distance between the beads containing the phosphorus atoms. For a pure DMPC bilayer, we obtained a bilayer thickness of 38.7 Å for the mesoscopic and 36.1 Å for the all-atom simulations. These data compare well with the experimental value of 36 Å.[52] Both experiments and simulations show a strong swelling of the bilayer thickness when up to 20−30 mol % cholesterol is added. This increase levels off when more cholesterol is added to the bilayer.

The effect of cholesterol on the ordering of the lipid tails is illustrated in Figure 3c. In the experiments, the lipid tail order parameter, S_{NMR}, is obtained from deuterium NMR experiments and is related to the average angle θ, between a C−D bond and the normal to the bilayer, by $S_{NMR} = 2|S_{CD}| = |\langle 3\cos^2\theta - 1\rangle|$. From all-atom simulations, one can directly obtain this NMR order parameter. The average angle β between a C−C bond and the normal to the bilayer is geometrically related to the desired angle θ. Hence, $2|S_{CD}|$ and $2|S_{CC}| = |\langle 3\cos^2\beta - 1\rangle|$ are expected to follow the same qualitative trend. We tested and validated this with our all-atom simulations (see Figure 3c). Therefore we use $2S_{TT} = |\langle 3\cos^2\alpha - 1\rangle|$ as the tail order parameter in our mesoscopic simulation, with α being the angle between two consecutive tail beads and the bilayer normal. Both all-atom molecular simulations and mesoscopic simulations reproduce the experimentally observed increase in lipid tail order when cholesterol is added to the bilayer, although the agreement is quantitatively better for all-atom molecular simulations.

The experimental data allow us to validate our model through various structural properties. It does not, however, allow us to validate the specific molecular organization of the lipids. To this end, we use the comparison to all-atom simulations. Figure 4 compares the density profiles of the cholesterol and DMPC head groups in the mesoscopic bilayer with all-atom simulations at various cholesterol concentrations. The comparison shows that our mesoscopic model follows the atomistic density profiles reasonably well, considering the loss of degrees of freedom by coarse-graining. The figure clearly shows the swelling of the bilayer induced by increasing concentration of cholesterol, as the head groups move increasingly away.

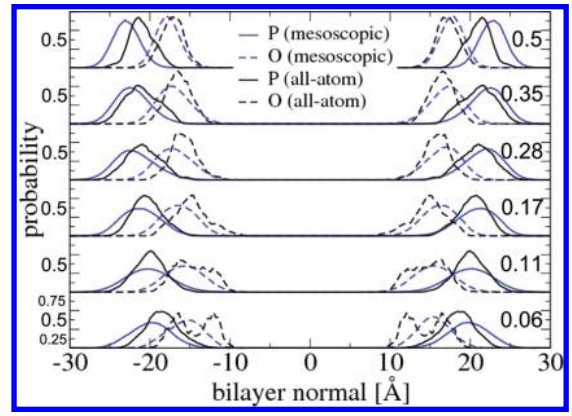

Figure 4. Comparison of the probability density distribution functions of the all-atom simulations (black lines) with the distribution functions from the coarse-grained simulations (blue lines) for different cholesterol mole fractions at $T = 30$ °C. The data are shifted three units along the vertical axis for increasing cholesterol concentration. In the comparison, we focus on the lipid phosphorus atom (solid lines) and the cholesterol oxygen atom (dashed lines). For the mesocopic simulations, we plot the density distribution of the lipid head bead containing the phosphorus atom (middle head bead) and the cholesterol bead containing the oxygen. The cholesterol mole fractions are given by the numbers on the right side of the graph.

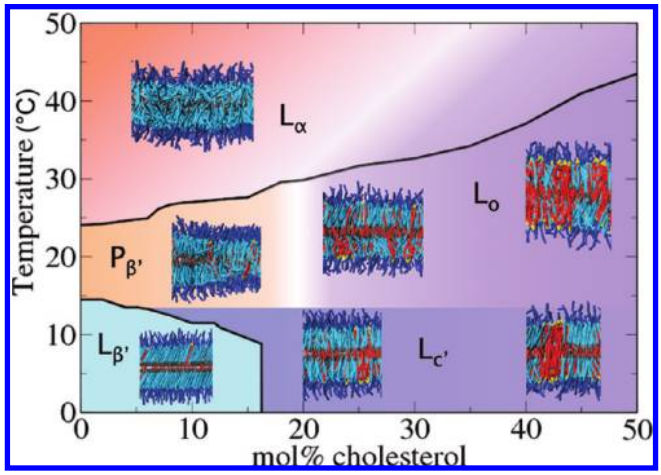

Figure 5. Temperature−composition structure diagram of the DMPC−cholesterol bilayer. The full lines were determined using inflection points of order parameters of the phase transition. All other regions are characterized via visual inspection of the snapshots, some of which are shown in the figure. Lipid head and tail beads are depicted in dark and light blue, respectively. The lipid tail end bead is depicted in gray. The cholesterol hydrophilic and hydrophobic beads are depicted in yellow and red, respectively. The snapshots were taken at the following conditions: $T = 35$ °C, pure DMPC (L_α phase); $T = 20$ °C, 10 mol % cholesterol ($P_{\beta'}$ phase); $T = 10$ °C, 5 mol % cholesterol ($L_{\beta'}$ phase); $T = 30$ °C, 30 mol % cholesterol (L_o phase, left); $T = 30$ °C, 50 mol % cholesterol (L_o phase, right, with random cholesterol clusters); $T = 10$ °C, 15 mol % cholesterol (L_c' phase, left); $T = 10$ °C, 50 mol % cholesterol (L_c' phase, right, with pure cholesterol patterns). The background colors depict the different phases, and the broadness of the transition between different colors represents the broadness of the transitions.

Mechanical. Figure 3d shows the relative area compressibility κ_A/κ_{A0} and bending modulus κ_C/κ_{C0}. The area compressibility was computed using $\kappa_A = k_B T A_t/(\delta A_t^2)$,[53] with A_t being the total bilayer area and (δA_t^2) being the mean square of the fluctuations in the area. Given the large scatter in the experimental values (144 ± 10.5[54] and 234 ± 23 dyn/cm[55]), our result for pure DMPC, $\kappa_A = 250 \pm 50$ dyn/cm, compares reasonably well. We predict a strong decrease in area fluctuations (δA_t^2) when cholesterol is added and thus a strong increase in area compressibility, in agreement with experimental observations.[54] To estimate the effect of cholesterol on the bending modulus, κ_C, we use the polymer brush model which relates κ_A to κ_C: $\kappa_C = (1/24)\kappa_A(PtP - 10\ \text{Å})^2$.[55] For pure DMPC, we compute $\kappa_C = 7.5 \pm 2 \times 10^{-20}$ J, which is of the same order of magnitude as the experimental value of $5-6 \times 10^{-20}$ J.[7,55] Our model correctly reproduces the increase in bending modulus due to the addition of cholesterol.

From this comparison of our mesoscopic model with experimental and all-atom simulation data, we can conclude that our very simple model reproduces, almost quantitatively, most structural and mechanical properties of DMPC. At this point, it is important to mention that we have also computed the diffusion coefficients for this model. As can be expected, due to the soft-repulsive interaction, these diffusion coefficients are 2−3 orders of magnitude larger compared to experimental values.

Temperature Dependence of the Structural and Mechanical Properties. The bilayer structural and mechanical properties strongly depend on the temperature and the composition. In addition, we can distinguish different bilayer structures at different temperatures and compositions. Figure 5 summarizes the phase behavior of our mesoscopic system. In this text we also call the different bilayer structures phases. Here we briefly describe the different bilayer structures to facilitate the interpretation of the temperature dependence of the mechanical and structural properties of the membrane. In a later section, we outline in detail how this phase diagram is obtained.

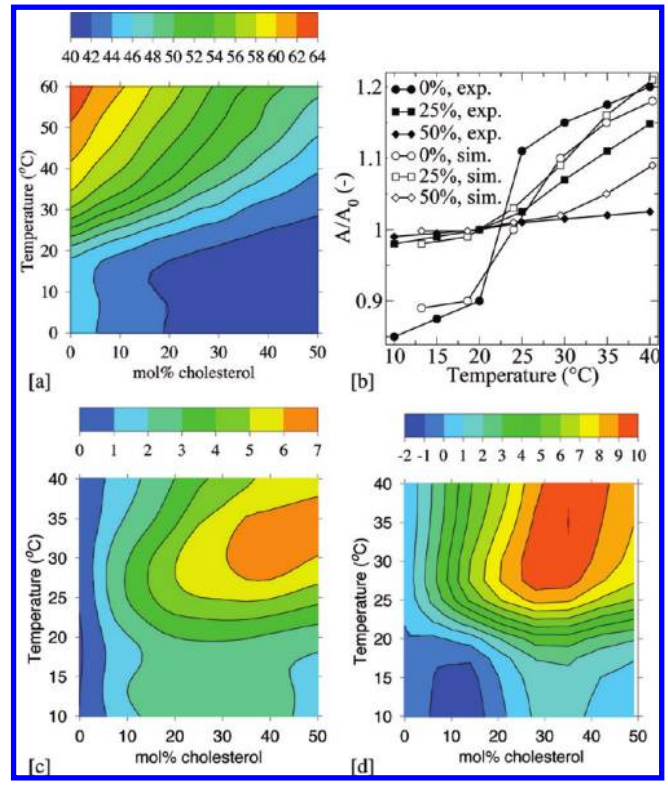

Figure 6. (a) Area per molecule, in Å^2, simulated with the mesoscopic model as a function of temperature and cholesterol concentration. (b) Comparison of the relative areas of bilayers containing 0, 25, and 50 mol % cholesterol, as a function of temperature, obtained from heating/cooling micropipet experiments by Needham et al.[54] and from our mesoscopic simulations. For the pure DMPC bilayer, A_0 is the area at the main transition temperature. For bilayers containing 25 and 50 mol % cholesterol, A_0 is the area at 20 °C. (c) Simulated condensation effect, in Å^2, defined as the difference between A_M simulated with the mesoscopic model and A_M^{IM} calculated according to the ideal mixing rule, as a function of temperature and cholesterol concentration. (d) Experimental condensation effect estimated from the relative areas reported by Needham et al.[54] and absolute areas reported by Hung et al.[52]

For a pure DMPC bilayer, we observed a disordered structure at high temperatures (L_α, or liquid phase), a rippled structure at intermediate temperatures ($P_{\beta'}$), and a tilted and ordered structure at lower temperatures ($L_{\beta'}$, or gel phase).

At high temperatures, we observed that the disordered bilayer structure gradually becomes more ordered when cholesterol is added to the bilayer. This ordered structure is called the L_o phase. As temperature increases, the cholesterol concentration at which the L_o phase is formed increases as well. At intermediate temperatures, we observe a transition from the $P_{\beta'}$ to the L_o phase. At low temperatures, the addition of cholesterol results in a nontilted highly ordered structure, called the L_c' phase. Larger snapshots of different bilayer structures are shown in the Supporting Information.

Structural. Similar to the validation at 30 °C, we computed the area per molecule, the bilayer thickness, and the lipid tail order and tilt as a function of temperature and bilayer composition.

Area per Molecule. A_M as a function of the bilayer composition and temperature is shown in Figure 6a. In this figure, isolines connect points with the same value of A_M. At high

temperatures, the bilayer is in the liquid L_α phase, where the tails are disordered and have the highest value of A_M. A_M decreases significantly if the temperature is decreased. As cholesterol occupies a smaller area ($A_{Chol,0} = 40.3$ Å^2), the addition of cholesterol decreases A_M. Addition of cholesterol decreases the temperature dependence of A_M. At low temperatures, in the gel phase, the effect of cholesterol on the area is much weaker.

Needham et al.[54] used micropipet aspiration of giant unilamellar vesicles to determine changes in area as a function of temperature (see Figure 6b). Needham et al. report a typical S-shape with a sudden decrease in bilayer area around the main transition temperature T_M. This S-shape is also reproduced by our simulations, although less steep. When 25 mol % cholesterol is added to the bilayer, the S-shape in the experimental curve disappears; the transition area is much smaller; and below T_M the temperature hardly affects the area anymore. As the cholesterol concentration is further increased to 50 mol %, the experimental curve shows no S-shape anymore and becomes almost flat. Our simulations nicely reproduce this experimental trend.

Condensation Effect. An interesting property of cholesterol is its condensation effect.[32,52,56] Cholesterol causes the area per molecule to decrease much more than one would expect on the basis of ideal mixing: $A_M^{IM} = (1 - x)A_{pc,0} + xA_{Chol,0}$, where $A_{pc,0}$ and $A_{Chol,0}$ are the area per pure lipid and cholesterol, respectively.

Figure 6c shows the influence of the temperature on the condensation effect. At low cholesterol concentrations, the condensation effect is small and does not depend on temperature. We find a strongly condensed region above the main transition of pure DMPC for cholesterol concentrations above 20 mol %. This condensation gap has not been measured directly. Interestingly, one can find indirect proof of this gap by combining the relative area measurements of Needham et al.[54] with the absolute values of A_m obtained by Hung et al.[52] Figure 6d shows a clear condensation gap for these combined data at conditions similar to our mesoscopic model. Quantitatively, the experimental maximum condensation effect is about 4 Å^2 higher than simulated and located at lower cholesterol concentrations, indicating that our model slightly underestimates the strength of the condensation effect. Apart from this, the agreement is surprisingly good. A detailed discussion on the mechanisms of the condensation effect has been the focus of a previous paper,[32] in which, however, we did not make the comparison with the experimental data.

Bilayer Thickness. In Figure 7a the relative bilayer thickness, defined as the phosphorus to phosphorus (PtP) distance divided by the PtP distance of pure DMPC at 30 °C, is shown as a function of temperature and cholesterol content for the DMPC−cholesterol bilayer. The behavior is similar to the area per molecule. For pure DMPC, we observe a strong temperature dependence around T_M. The addition of cholesterol smoothens out the temperature dependence of the bilayer thickness. At high temperatures, cholesterol increases the bilayer thickness, while at low temperatures, cholesterol does not affect the bilayer thickness much. Thus, the bilayer thickness depends on the relative importance of two different effects: the swelling of the bilayer when the temperature is decreased and the swelling of the bilayer when cholesterol is added.

Few experimental data are available for the bilayer thickness, and the effect of cholesterol on the bilayer thickness is still subject to debate. The main transition of a pure DMPC bilayer is accompanied by a sudden increase in bilayer thickness, and small amounts of cholesterol do not seem to influence this bilayer swelling significantly.[57] This is confirmed by our simulation results. Also, it was observed for a DPPC−cholesterol bilayer that, above 25 mol % cholesterol, the bilayer is thicker in the fluid phase and thinner in the gel phase than the pure DPPC bilayer.[58] This is exactly what we compute. Several studies such as the neutron diffraction study of Léonard et al.[59] mention an increase of the hydrophobic thickness by 3−4 Å when cholesterol is added to the DMPC bilayer, independent of the temperature. We clearly simulate a cholesterol dependence of the hydrophobic thickness that does also depend on the temperature. It was also recently reported that the cholesterol-induced bilayer swelling is not observed in vivo.[60]

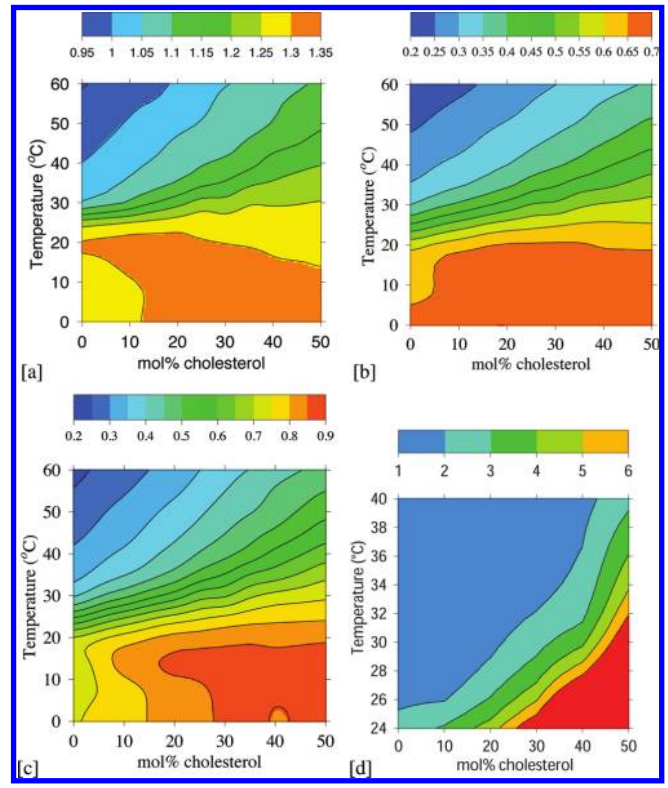

Figure 7. (a) Bilayer thickness, relative with respect to the cholesterol-free bilayer thickness at 30 °C, as a function of cholesterol concentration and temperature, in °C. (b) Average lipid tail order (S_{TT}). (c) Lipid tail tilt (S_{T1T4}). (d) Membrane bending modulus, relative with respect to the cholesterol-free membrane modulus at 30 °C.

Lipid Tail Order and Tilt. The average tail order parameter is shown in Figure 7b as a function of the bilayer composition and the temperature for the DMPC−cholesterol mixture. At high temperatures, the average order of the lipid tails increases steadily when cholesterol is added to the bilayer. At low temperatures, cholesterol does not really seem to affect the order parameter much. At intermediate temperatures, the lipid tail order increases up to a given cholesterol concentration after which it remains rather constant.

The temperature and composition dependence of the average tail tilt is quite similar. This is shown in Figure 7c. The only qualitative difference is that at low temperatures cholesterol concentrations ranging from 0 to 30 mol % also increase the tilt parameter, which corresponds to a decrease in lipid tail tilt. The tilt parameter is defined as $2S_{T1T4} = |\langle 3\cos^2\alpha - 1\rangle|$, with α being the angle between the first and the last tail beads and the bilayer normal.

Systematic qualitative experiments have been performed by Wilson-Ashworth et al.[61] for the DPPC−cholesterol mixture. Their results can be summarized as follow: above the main phase

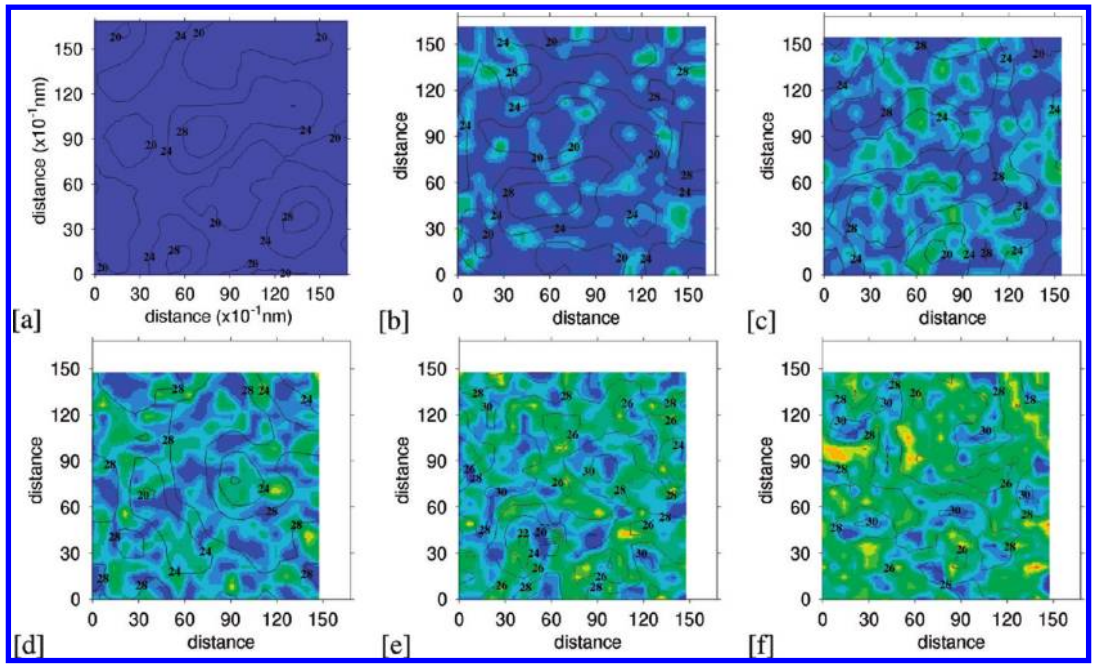

Figure 8. Hydrophobic thickness variation, in Å, and local mole fractions, for $T = 30$ °C, at various cholesterol concentrations (0 (a), 10 (b), 20 (c), 30 (d), 40 (e), 50 (f)). The figure shows a top view of the bilayer in which the lines and numbers give the thickness and the colors the local cholesterol concentration. Blue indicates that both layers contain only lipids, and red indicates that both layers contain a cholesterol. The axes are in Å.

transition temperature, cholesterol induces an ordering, which is comparable to the order of pure DPPC between the main and the pretransition temperature. Between the main and the pretransition temperature, cholesterol induces ordering comparable to the order of the pure DPPC below the pretransition temperature. Below the pretransition temperature cholesterol does not seem to affect the order. Qualitatively this is exactly what we simulate.

The ordering effect of cholesterol above T_M is agreed upon in the literature. This is not the case for the ordering effect of cholesterol below T_M. Shimshick et al.[62] report a slight increase of the average tail order parameter with increasing cholesterol concentration, at temperatures below T_M. The lower the temperature, the smaller the cholesterol range over which the biggest increase of S_{NMR} occurs. This is not in agreement with the results of Ipsen et al.,[63] who report a decreasing order parameter with increasing cholesterol concentration.

In a DMPC−cholesterol and a DPPC−cholesterol mixture, a phase was observed below the pretransition temperature T_P where the lipid chains are less tilted than in the L_β' phase.[64,65] Karmakar et al.[65] called this phase the P_β phase. However, experimentally, no agreement has been reached over the exact cholesterol content interval over which this phase occurs. Karmakar et al.[65] mention a pure L_β' phase up to 2 mol % cholesterol, a coexistence of L_β' and P_β between 2 and 13 mol % cholesterol, and a pure P_β phase between 13 and 21 mol % cholesterol. Knoll et al.[64] observe a strong decrease of the lipid tail tilt between 8 and 24 mol % cholesterol. In our simulations, for a pure DMPC bilayer, the value of the tilt parameter in the L_β' is around 0.71, corresponding with a tilt of approximately 26°, which compares well with the most recent experimental estimate of 32.3°.[66] Between 0 and 25 mol % cholesterol the value of the tilt parameter increases up to 0.9, corresponding with a tilt angle of of approximately 15°. Thus, our model correctly predicts the decrease in tilt in the gel phase due to the addition of cholesterol.

Mechanical. Figure 7d shows the membrane bending modulus, relative to the cholesterol-free membrane modulus at 30 °C, as a function of the composition, and over the temperature range 24−40 °C, i.e., above the main transition temperature of DMPC, which is 24 °C. In this temperature range, the bending modulus of DMPC is hardly temperature-dependent. At a constant temperature of, for example, 26 °C, addition of cholesterol results in an increase of the bilayer bending modulus. For example, 30 mol % cholesterol multiplies the bending modulus by a factor of 5. With increasing temperature, however, this effect of cholesterol strongly decreases, and at 40 °C the addition of 40 mol % cholesterol multiplies the bending modulus only by a factor of 2. This is in good agreement with the factor 2.5, measured experimentally by Meléard et al.[67] This is shown in Figure 3d.

Temperature Dependence of the Lateral Organization of Cholesterol. In Figures 8−10, the bilayer hydrophobic thickness variations and the local cholesterol concentrations are shown at various cholesterol concentrations for different temperatures. The lateral organization of cholesterol is difficult to measure experimentally but is important for the interpretation of some experiments and for the modeling of cholesterol−lipid interactions.[12]

At $T = 30$ °C (Figure 8), when pure DMPC is well in the liquid phase, there are only small and local variations in bilayer thickness. This remains so when cholesterol is added to the bilayer. There are very small regions with and without cholesterol. Dips in the fluorescence intensity as a function of cholesterol concentration have often been presented as evidence for a regular distribution of cholesterol on a fixed hexagonal superlattice in DMPC bilayers. This regular distribution implies that every cholesterol molecule has a preferential location in the plane of the membrane with respect to the other cholesterol molecules. A dip is observed at, for example, 20 mol % cholesterol.[68−70] However, we could not observe any form of regular cholesterol distribution in our simulations. At higher cholesterol concentrations, i.e., when the bilayer is in the liquid-ordered phase, small dynamical cholesterol clusters are present.

Experimentally, it would be very difficult to detect such small cholesterol clusters. From the analysis of fluorescence resonance

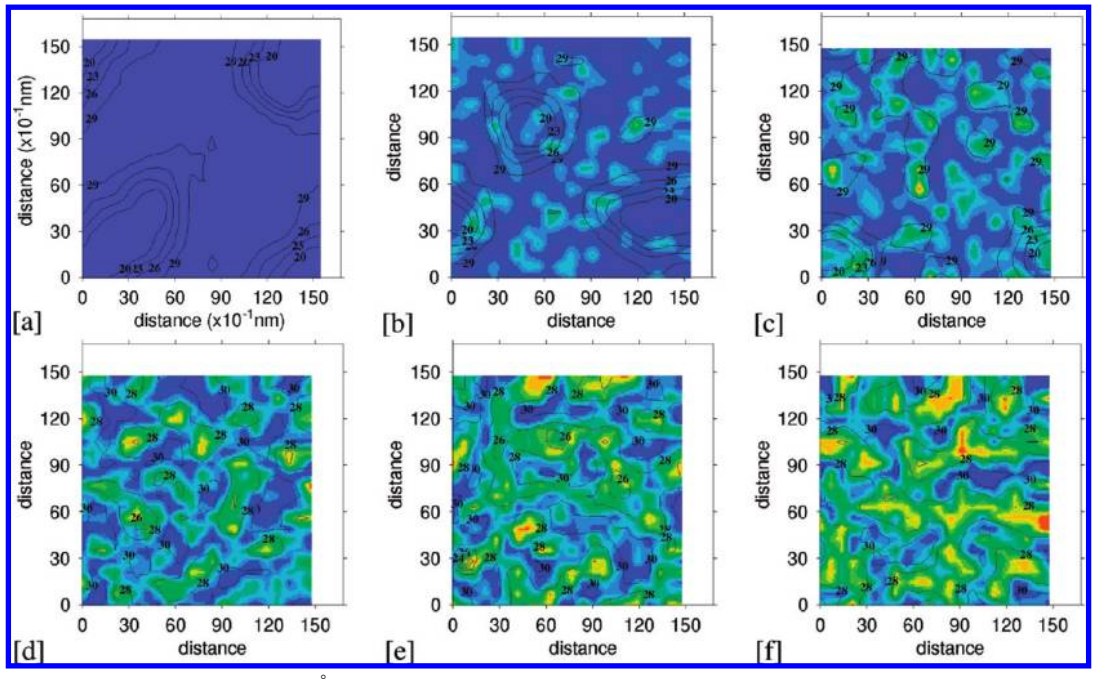

Figure 9. Hydrophobic thickness variation, in Å, and local cholesterol mole fractions, for $T = 21$ °C, at various cholesterol concentrations (0 (a), 10 (b), 20 (c), 30 (d), 40 (e), 50 (f)).

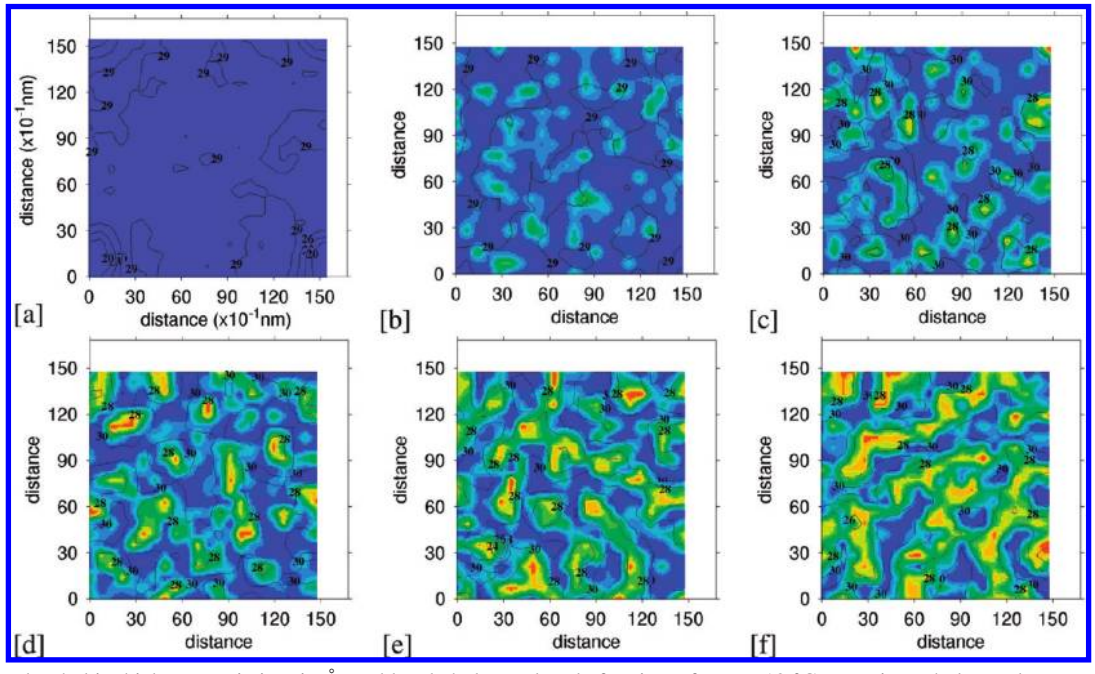

Figure 10. Hydrophobic thickness variation, in Å, and local cholesterol mole fractions, for $T = 10$ °C, at various cholesterol concentrations (0 (a), 10 (b), 20 (c), 30 (d), 40 (e), 50 (f)).

energy transfer data, Troup et al.[71,72] concluded that cholesterol clusters exist in the DMPC bilayer with 40 mol % cholesterol, above the main phase transition temperature of pure DMPC. Using all-atom simulations, Dai et al.[12] did not observe clustering of cholesterol, but their cholesterol content was never higher than 20 mol % cholesterol. It might well be that part of the cholesterol clustering we observe is related to the slight underestimation of the cholesterol condensation effect.

At $T = 21$ °C (Figure 9), the hydrophobic thickness variations (20 Å for the thin and 29 Å for the thick part) illustrate the ripple phase at 0% cholesterol. Due to the addition of cholesterol, the ripples gradually disappear. In the rippled phase, there seems to be a slight preference of cholesterol for the thicker bilayer domains. In the liquid-ordered phase, small dynamical cholesterol clusters appear. The disappearance of the ripple phase around 20 mol % cholesterol and the preference of cholesterol for the thicker bilayer domains is in agreement with the experimental observations of Mortensen et al.[73]

At $T = 10$ °C (Figure 10), the pure DMPC bilayer is well in the gel phase. At high cholesterol concentrations, cholesterol forms larger clusters. It is also more likely to find a cholesterol molecule in both layers at the same position.

Temperature−Composition Structure Diagram. Ideally, one would use a change in the enthalpy as a signature for a phase transition. However, for our system, molecular simulations of the heat capacity signature of DSC experiments are very difficult due to the large bulk water contribution. As an alternative, we used order parameters of the phase transition,

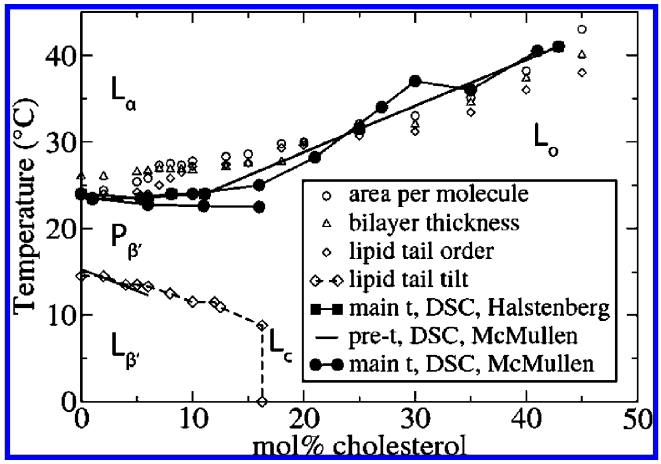

Figure 11. Effect of cholesterol on the main and the pretransition temperature of a DMPC bilayer. The experimental data were obtained from differential scanning calorimetry by Halstenberg et al.[4] and from deconvolution of the main transition temperature DSC peak by McMullen et al.[5] The open symbols are the results of the simulations using the temperature−composition position of the inflection points of the curves representing the values of the area per molecule, lipid tail order, lipid tail tilt, and bilayer thickness as a function of temperature, at a given cholesterol concentration.

which are parameters of which the value significantly changes during a phase transition. For this system, the area per molecule, the bilayer thickness, and the tail order and tilt parameters were considered as order parameters of a phase transition. We defined the inflection points of the curves of the temperature dependence of the order parameters as the boundaries between the phases. For pure DMPC, heating and cooling simulations were performed to check the reversibility of the phase transitions. The rate of heating and cooling was 1 °C per simulation. For the main transition, no hysteresis was observed, while for the pretransition, a slight hysteresis ($\Delta T = \pm 1$ °C) was present. For the DMPC−cholesterol bilayers, only cooling simulations were performed. For the transitions $L_\alpha \rightarrow P_\beta'$, $L_\alpha \rightarrow L_o$, $P_\beta' \rightarrow L_\beta'$, and $L_c' \rightarrow L_\beta'$. we could observe a clear inflection point (see Supporting Information). All other regions were identified by visual inspection of the snapshots.

Figure 11 collects the inflection points of these different order parameters as a function of cholesterol composition (the complete curves can be found in the Supporting Information). Within the accuracy at which these inflections points can be determined, all order parameters give similar results. At low cholesterol concentrations, we observed a relatively sharp inflection. For concentrations above 20% cholesterol, this transition became much more gradual. For the $L_\alpha \rightarrow P_\beta'$ and $L_\alpha \rightarrow L_o$ transitions, our data nicely follow the DSC experiments by Halstenberg et al.[4] and McMullen et al.[5] The temperature at which the heat capacity peak is maximal remains approximately constant until 10−15 mol % cholesterol is added, after which the temperature increases. At 15 mol % cholesterol, the DSC peak broadens; a gradual transition or a crossover to the L_o phase takes place; and the main transition enthalpy approaches zero between 40 and 45 mol % cholesterol. Also, for the pretransition, our results are in very good agreement with the DSC experiments of McMullen et al.[5]

It is instructive to compare our phase diagram (Figure 5) with the experimental ones shown in Figure 1. The effect of cholesterol on T_M in the structure diagram of Recktenwald et al.[74] (see Figure 1b), obtained with fluidity measurements, is very similar to the effect observed by the DSC experiments and our simulations. In contrast, the structure diagram of Mortensen et al.[73] (Figure 1a) shows a slight decrease of the temperature of the transition from the L_α to the P_β' structure, up to 20 mol % cholesterol.

The DPPC−cholesterol phase diagrams[58,75−78] show some qualitative agreement with the DMPC−cholesterol diagrams.[5] In fact, for our mesoscopic model the difference in tail length between DMPC and DPPC is too small to be described by the addition or removal of an extra tail bead. Vist et al.[58] (Figure 1c) observed a decrease of the main phase transition up to 8 mol % cholesterol, followed by a liquid−liquid immiscible region. We do not observe such a liquid−liquid immiscibility gap. However, the gradual transition of the L_α to the L_o phase might explain the broadening of the NMR signal.[58] Recent X-ray scattering experiments also concluded that liquid−liquid immiscibility is not present in the DPPC−cholesterol system.[79]

Below the main-transition temperature, the addition of cholesterol induces a gradual transition from a P_β' to an L_o phase. Our mesoscopic simulations indicate that the ripple phase exists up to 20 mol % cholesterol, in agreement with the experiments of Mortensen et al.[73] (see Figure 1a). Vist et al.[58] (Figure 1c) observe the coexistence of gel and the L_o phase; however, recent X-ray scattering experiments concluded that gel−L_o immiscibility is not present in the DPPC−cholesterol system.[79] We do not find evidence from our simulations for this coexistence. It might be that the change in NMR signal, which lead Vist et al.[58] to conclude that immiscibility of two phases might be present, is due to the presence of small ripples, as observed in our simulations. The term liquid-ordered phase was introduced[80] because it was experimentally observed that, although the lipid tails in the L_o phase were highly ordered, the diffusion coefficient was, although lower, still of the same order of magnitude as in the L_α phase,[10] and surface shear rigidity was absent.[54] The DSC experiments and our simulations show that cholesterol increases the $L_\alpha \rightarrow L_o$ transition temperature, which is a natural continuation of the main phase transition line, with the L_o phase at the gel-side of the crossover.

As mentioned previously, DSC experiments indicate that the pretransition temperature decreases when up to 6 mol % cholesterol is added and thereafter disappears. The pretransition, as obtained from DSC experiments, is interpreted as the transition from the P_β' to the L_β' phase.[77] Above 6 mol % cholesterol, no significant change in enthalpy was observed. If we compare this with our phase diagram, at approximately these conditions we observe a transition from the P_β' to the L_β' and a transition from the L_β' to the L_c' phase. In the L_β' phase, we observe that the tilt order decreases as a function of temperature, while in the L_c' phase the tilt order increases. This behavior gives a very interesting temperature dependence at 10 mol %, in which we observed three inflection points (see Supporting Information for more details). The simulated L_c' phase, in which the lipid chains are less tilted than in the L_β' phase, was also experimentally observed.[64,79]

Concluding Remarks

In this work we have introduced a very simple model of a phospholipid and cholesterol. In this model, cholesterol is characterized by a bulky hydrophobic core, a small hydrophilic head, and a small hydrophobic tail. These ingredients give our model of cholesterol many unique properties. Our model agrees well with experimental data on structural and mechanical properties of the bilayer, as well as with all-atom simulations. This agreement coupled with the reproduction of many experimentally observed DMPC−cholesterol structural and mechanical properties indicates that our model captures the essence of

DMPC−cholesterol mixing. The temperature−composition dependence of the lateral organization of cholesterol might give important information for the correct interpretation of experiments.

For most thermodynamic systems, the addition of a second component induces disorder into the system. The addition of cholesterol, however, causes the lipid molecules to order. Our simulations show that this effect strongly depends on temperature. At very high temperature, the membrane can accommodate a significant amount of cholesterol without structural changes. At low temperatures, cholesterol induces different phases in which the lipid tails are more ordered. Such a more ordered structure allows the lipids to support cholesterol by reducing the water hydrophobic contacts. In this context one can understand the role of the bulky hydrophobic core and the relatively small hydrophilic head.

The main result of the work is the phase diagram shown in Figure 5. We have argued that one can find experimental evidence for most of these phases. However, more importantly our model calculations provide a rationale for why the "true" experimental phase diagram is not known. The simulations show that cholesterol induces many subtle structural changes, which may or may not be observable for different experimental techniques. Reflecting the simplicity of the model, we obtain general insights which may help experimentalists interpret their phase diagrams.

Acknowledgment. F. de Meyer and A. Benjamini are supported by the Laboratory Directed Research and Development Program of Lawrence Berkeley National Laboratory under the Department of Energy Contract No. DE-AC02-05CH11231. J. Rodgers is supported by the Chemical Sciences, Geosciences and Biosciences Division, Office of Basic Energy Sciences, Office of Science, U.S. Department of Energy, FWP number SISGRKN.

Note Added after ASAP Publication. This paper was published on the Web on July 26, 2010. Revisions were made to Figures 8a, 9a, and 10a. The corrected version was reposted on July 28, 2010.

Supporting Information Available: The DPD-MC simulation method is explained in more detail. The simulation data of the atomistic and the mesoscopic simulations are also available, as well as a detailed derivation of the phase boundaries and some snapshots of the bilayers. This material is available free of charge via the Internet at http://pubs.acs.org.

References and Notes

(1) Oldfield, E.; Chapman, D. *FEBS Lett.* **1972**, *23*, 285–297.
(2) McMullen, T. P. W.; Lewis, R. N. A. H.; McElhaney, R. N. *Curr. Opin. Colloid Interface Sci.* **2004**, *8*, 459–468.
(3) Heimburg, T. *Thermal biophysics of membranes*, 1st ed.; Wiley-VCH: Weinheim, 2007.
(4) Halstenberg, S.; Heimburg, T.; Hianik, T.; Kaatze, U.; Krivanek, R. *Biophys. J.* **1998**, *75*, 264–271.
(5) McMullen, T. P. W.; Lewis, R. N. A. H.; McElhaney, R. N. *Biochemistry* **1993**, *32*, 516–522.
(6) Mills, T. T.; Toombes, G. E. S.; Tristram-Nagle, S.; Smilgies, D. M.; Feigenson, G. W.; Nagle, J. *Biophys. J.* **2008**, *21*, 669–681.
(7) Pan, J.; Mills, T. T.; Tristram-Nagle, S.; Nagle, J. F. *Phys. Rev. Lett.* **2008**, *100*, 198103 1–4.
(8) Pan, J.; Tristram-Nagle, S.; Nagle, J. F. *Phys. Rev. E* **2009**, *80*, 021931−021943.
(9) Filippov, A.; Orädd, G.; Göran, L. *Biophys. J.* **2003**, *84*, 3079–3086.
(10) Rubenstein, J. L. R.; Smith, B. A.; McConnell, H. M. *Proc. Natl. Acad. Sci. U.S.A.* **1979**, *76*, 15–18.
(11) Almeida, P. F. F.; Vaz, W. L. C.; Thompson, T. E. *Biochemistry* **1992**, *31*, 6739–6747.
(12) Dai, J.; Alwarawrah, M.; Huang, J. *J. Phys. Chem. B* **2010**, *114*, 840–848.
(13) Róg, T.; Pasenkiewicz-Gierula, *FEBS Lett.* **2001**, *502*, 68–71.
(14) Chiu, S. W.; Jakobsson, E.; Mashl, R. J.; Scott, H. L. *Biophys. J.* **2002**, *83*, 1842–1853.
(15) Niemela, P. S.; Hyvonen, M. T.; Vattulainen, I. *Biochim. Biophys. Acta* **2009**, *1788*, 122–135.
(16) Kucerka, N.; Perlmutter, J. D.; Pan, J.; Tristram-Nagle, S.; Katsaras, J.; Sachs, J. N. *Biophys. J.* **2008**, *95*, 2792–2805.
(17) Pandit, S. A.; Bostick, D.; Berkowitz, M. L. *Biophys. J.* **2004**, *86*, 1345–1356.
(18) Cournia, Z.; Ullmann, G. M.; Smith, J. C. *J. Phys. Chem. B* **2007**, *111*, 1786–1801.
(19) Smondyrev, A. M.; Berkowitz, M. L. *Biophys. J.* **1999**, *77*, 2075–2089.
(20) Smondyrev, A. M.; Berkowitz, M. L. *Biophys. J.* **2001**, *80*, 1649–1658.
(21) Pasenkiewicz-Gierula, M.; Róg, T.; Kitamura, K.; Kusumi, A. *Biophys. J.* **2000**, *78*, 1376–1389.
(22) Róg, T.; Pasenkiewicz-Gierula, M. *Biophys. Chem.* **2004**, *107*, 151–164.
(23) Berkowitz, M. L. *Biochim. Biophys. Acta* **2009**, *1788*, 86–96.
(24) Bennett, W. F. D.; MacCallum, J. L.; Hinner, M. J.; Marrink, S. J.; Tieleman, D. P. *J. Am. Chem. Soc.* **2009**, *131*, 12714–12720.
(25) Hofsass, C.; Lindahl, E.; Edholm, O. *Biophys. J.* **2003**, *84*, 102–115.
(26) Venturoli, M.; Sperotto, M. M.; Kranenburg, M.; Smit, B. *Phys. Rep.* **2006**, *437*, 1–57.
(27) Groot, R. D.; Warren, P. B. *J. Chem. Phys.* **1997**, *107*, 4423–4435.
(28) Lenz, O.; Schmid, F. *Phys. Rev. Lett.* **2007**, *98*, 058104−058108.
(29) Izvekov, S.; Voth, G. A. *J. Chem. Theory Comput.* **2006**, *2*, 637–648.
(30) Murtola, T.; Karttunen, M.; Vattulainen, I. *J. Chem. Phys.* **2009**, *131*, 055101−055115.
(31) Marrink, S. J.; Risselada, H. J.; Yefimov, S.; Tieleman, D. P.; de Vries, A. H. *J. Phys. Chem. B* **2007**, *111*, 7812–7824.
(32) de Meyer, F.; Smit, B. *Proc. Natl. Acad. Sci. U.S.A.* **2009**, *106*, 3654–3658.
(33) Cao, H.; Tokutake, N.; Regen, S. L. *J. Am. Chem. Soc.* **2003**, *125*, 16182–16183.
(34) Huang, J. *Biophys. J.* **2002**, *83*, 1014–1025.
(35) Ali, M. R.; Cheng, K. H.; Huang, J. *Proc. Natl. Acad. Sci. U.S.A.* **2007**, *104*, 5372–5377.
(36) Brzozowska, I.; Figaszewski, Z. A. *Colloids Surf., B* **2002**, *23*, 51–58.
(37) Bernsdorff, C.; Winter, R. *J. Phys. Chem. B* **2003**, *107*, 10658–10664.
(38) Gao, W. Y.; Quinn, P. J.; Yu, Z. W. *Mol. Membr. Biol.* **2008**, *25*, 485–497.
(39) Hoogerbrugge, P. J.; Koelman, J. M. V. A. *Europhys. Lett.* **1992**, *19*, 155–160.
(40) Español, P.; Warren, P. B. *Europhys. Lett.* **1995**, *30*, 191–196.
(41) Marrink, S. J.; Lindahl, E.; Edholm, O.; Mark, A. E. *J. Am. Chem. Soc.* **2001**, *123*, 8638–8639.
(42) Kranenburg, M.; Smit, B. *J. Phys. Chem. B* **2005**, *109*, 6553–6563.
(43) Venturoli, M.; Smit, B.; Sperotto, M. M. *Biophys. J.* **2005**, *88*, 1778–1798.
(44) de Meyer, F. J.-M.; Venturoli, M.; Smit, B. *Biophys. J.* **2008**, *95*, 1851–1865.
(45) Rodgers, J. M.; Webb, M.; Smit, B. *J. Chem. Phys.* **2010**, *132*, 3437–3441.
(46) M'Baya, G.; Mely, Y.; Duportail, G.; Klymchenko, A. S. *Biophys. J.* **2008**, *95*, 1217–1225.
(47) Jo, S.; Kim, T.; Iyer, V. G.; Im, W. *J. Comput. Chem.* **2008**, *29*, 1859–1865.
(48) Jo, S.; Limm, J. B.; Klauda, J. B.; Im, W. *Biophys. J.* **2009**, *97*, 50–58.
(49) Brooks, B. R.; Bruccoleri, R. E.; Olafson, B. D.; States, D. J.; Swaminathan, S. *J. Comput. Chem.* **1983**, *4*, 187–217.
(50) Klauda, J. B.; Brooks, B. R.; MacKerell, A. D.; Venable, R. M.; Pastor, R. W. *J. Phys. Chem. B* **2005**, *109*, 5300–5311.
(51) Darden, T.; York, D.; Pederson, L. *J. Chem. Phys.* **1993**, *98*, 10089–10092.
(52) Hung, W.-C.; Lee, M.-T.; Chen, F.-Y.; Huang, H. W. *Biophys. J.* **2007**, *92*, 3960–3967.
(53) Orsi, M.; Haubertin, D. Y.; Sanderson, W. E.; Essex, J. W. *J. Phys. Chem. B* **2008**, *112*, 802–815.
(54) Needham, D.; McIntosh, T. J.; Evans, E. *Biochemistry* **1988**, *27*, 4668–4673.
(55) Rawicz, W.; Olbrich, K. C.; McIntosh, T. J.; Needham, D.; Evans, E. *Biophys. J.* **2000**, *79*, 328–339.
(56) Leathes, J. B. *Lancet* **1925**, *205*, 853–856.

(57) Lemmich, J.; Mortensen, K.; Ipsen, J. H.; Honger, T.; Bauer, R.; Mouritsen, O. G. *Eur. Biophys. J.* **1997**, *25*, 293–304.

(58) Vist, M. R.; Davis, J. H. *Biochemistry* **1990**, *29*, 451–464.

(59) Léonard, A.; Escrive, C.; Laguerre, M.; Pebay-Peyroula, E.; Néri, W.; Pott, T.; Katsaras, J.; Dufourc, E. *Langmuir* **2001**, *17*, 2019–2030.

(60) Mitra, K.; Ubarretxena-Belandia, I.; Taguchi, T.; Warren, G.; Engelman, D. M. *Proc. Natl. Acad. Sci. U.S.A.* **2004**, *101*, 4083–4088.

(61) Wilson-Ashworth, H. A.; Bahm, Q.; Erickson, J.; Shinkle, A.; Vu, M. P.; Woodbury, D.; Bell, J. *Biophys. J.* **2006**, *91*, 4091–4101.

(62) Shimschick, E. J.; McConnell, H. M. *Biochem. Biophys. Res. Commun.* **1973**, *53*, 446–451.

(63) Ipsen, J. H.; Mouritsen, O. G.; Bloom, M. *Biophys. J.* **1990**, *57*, 405–412.

(64) Knoll, W.; Schmidt, G.; Ibel, K.; Sackmann, E. *Biochemistry* **1985**, *24*, 5240–5346.

(65) Karmakar, S.; Raghunathan, V. A. *Phys. Rev. Lett.* **2003**, *91*, 098102−1−098102−4.

(66) Tristram-Nagle, S.; Liu, Y.; Legleiter, J.; Nagle, J. F. *Biophys. J.* **2002**, *83*, 3324–3335.

(67) Méleard, P.; Gerbeaud, C.; Pott, T.; Fernandez-Puente, L.; Bivas, I.; Mitov, M. D.; Dufourcq, J.; bothorel, P. *Biophys. J.* **1997**, *72*, 2616–2629.

(68) Chong, P. L.-G. *Proc. Natl. Acad. Sci. U.S.A.* **1994**, *91*, 10069–10073.

(69) Virtanen, J. A.; Ruonala, M.; Vauhkonen, M.; Somerharju, P. *Biochemistry* **1995**, *34*, 11568–11581.

(70) Tang, D.; Van Der Meer, W.; Chen, S.-Y. S. *Biophys. J.* **1995**, *68*, 1944–1951.

(71) Troup, G. M.; Tulenko, T. N.; Lee, S. P.; Wrenn, S. *Colloids Surf. B* **2003**, *29*, 217–231.

(72) Troup, G. M.; Tulenko, T. N.; Lee, S. P.; Wrenn, S. *Colloids Surf. B* **2004**, *33*, 57–65.

(73) Mortensen, K.; Pfeiffer, W.; Sackmann, E.; Knoll, W. *Biochim. Biophys. Acta* **1988**, *945*, 221–245.

(74) Recktenwald, D. J.; McConnell, H. M. *Biochemistry* **1981**, *20*, 4505–4510.

(75) Lentz, B. R.; Barrow, D. A.; Hoechli, M. *Biochemistry* **1980**, *19*, 1943–1954.

(76) Huang, T.-H.; Lee, C. W. B.; Das Gupta, S. K.; Blume, A.; Griffin, R. G. *Biochemistry* **1993**, *32*, 13277–13287.

(77) McMullen, T. P. W.; McElhaney, R. N. *Biochim. Biophys. Acta* **1995**, *1234*, 90–98.

(78) Clarke, J. A.; Heron, A. J.; Seddon, J. M.; Law, R. V. *Biophys. J.* **2006**, *90*, 2383–2393.

(79) Mills, T.; Huang, J.; Feigenson, G. W.; Nagle, J. *Gen. Physiol. Biophys.* **2009**, *28*, 126–139.

(80) Ipsen, J. H.; Karlström, G.; Mouritsen, O. G.; Wennerström, H.; Zuckermann, M. J. *Biochim. Biophys. Acta* **1987**, *905*, 162–172.

JP103903S